2010-03-15

The Control of Rotor Side and Grid Side Converters in a DFIG During Network Voltage Unbalance Conditions Using Resonant Current Controllers.

Joseph Kearney
Technological University Dublin, joseph.kearney@tudublin.ie

Michael Conlon
Technological University Dublin, michael.conlon@tudublin.ie

Eugene Coyle
Technological University Dublin, Eugene.Coyle@tudublin.ie

ECOLOGIC VEHICLES • RENEWABLE ENERGIES
MONACO
MARCH 25-28 2010

The Control of Rotor Side and Grid Side Converters in a DFIG During Network Voltage Unbalance Conditions Using Resonant Current Controllers.

Joe Kearney
Dublin Institute of Technology, Ireland
E-mail: Joseph.kearney@dit.ie

Michael Conlon
Dublin Institute of Technology, Ireland
E-mail: Michael.Conlon@dit.ie

Eugene Coyle
Dublin Institute of Technology, Ireland
E-mail: Michael.Conlon@dit.ie

Abstract: *This paper implements control techniques to enable improved operation of DFIG's when subjected to the effects of network voltage unbalance conditions. The control scheme involves the integration of a resonant regulator into the PI controllers of both the rotor side and grid side converters in a DFIG. The resonant controller is tuned to twice the network frequency ($2\omega_e$) and designed to mitigate against the power oscillations and torque pulsations in a DFIG due to network voltage unbalance conditions. The grid side converter controller also incorporates a second resonant controller tuned to three times the grid frequency ($3\omega_e$) to alleviate the amplitude of the generated third harmonic currents. The control schemes of both the rotor side and grid side converters are coordinated to enable concurrent reductions in both the torque pulsations and the total DFIG power oscillations. A DFIG model is implemented in the program Matlab/Simulink and simulations show the reduction in power and torque oscillations and a reduction in the high unbalanced currents generated as a result of the applied voltage unbalance.*

Keywords: DFIG, Voltage Unbalance, Wind Energy, Resonant Controller.

1. Introduction

Most recently installed wind energy conversions systems contain variable speed generators the most popular being the Double Fed Induction Generator (DFIG). DFIG's contain an induction generator, the stator of which is connected directly to the grid. The rotor of the induction generator is connected to a back-to-back converter and then to the grid. The main advantage of DFIG's in comparison to other variable speed generators is that for a similar power rating the converter in the rotor of the DFIG is normally sized according to the range of speed required. Most modern DFIG's operate with a speed range typically 30% of the rated speed of the induction generator and therefore the rotor converter can be sized to a value of 30% of the rated power of the induction generator.

In a DFIG both the stator and the rotor converter are connected directly to the grid and

thus any voltage problems on the network can affect both the induction generator and the rotor converter. Network voltage unbalance is a power quality problem that can affect wind turbines. Voltage unbalance can give rise to excessive unbalanced stator and rotor currents in Double Fed Induction Generators (DFIG's) and overloading of the rotor converter causing generators to trip out [8]. Mechanical stress can also occur due to torque pulsations.

This paper considers measures, which are available to alleviate the effects of voltage unbalance. The control scheme involves modifying the standard DFIG control structures of both the rotor side and grid converter and introducing a resonant controller to the PI control in the current loops of the DFIG. This control structure is implemented in both the rotor-side converter and the grid-side converters.

The methods used also integrate the control variables of both the rotor-side and grid-side converters in a coordinated fashion and show it is possible to reduce both the DFIG total power oscillations and torque pulsations. Improvements in the control structures of the rotor side and grid side converters are investigated, and simulations performed in Matlab/Simulink to outline the improvements in the performance of the DFIG.

2. Method of Controlling DFIG During Voltage Unbalance Conditions

The DFIG consists of an induction generator and a back-to-back PWM converter consisting of a rotor side and grid converter. Network voltage unbalance not only affects the induction generator but also the PWM converter in the rotor [[9]. The rotor side converter normally controls the real power and reactive power supplied to the network, whereas the grid side converter controls the dc link bus voltage and can also influence the power factor [1].

To reduce the power and torque pulsations as a result of network voltage unbalance it is necessary to modify the control structure of the rotor side converter. The traditional control structure of a DFIG can be modified to incorporate routines for positive and negative sequence control [4], [7], [9]. Power and torque oscillations can also be alleviated by using a resonant harmonic controller (R) in parallel with the PI controller in the control loop of the rotor side converter [13].

In an unbalanced network the stator apparent power can be expressed in terms of positive and negative sequence components [[4], [5], [6]]. Due to these components it is necessary to analyse the DFIG per-phase equivalent circuit in the positive and negative sequence *dq* reference frames.

3. Rotor Side Converter Control

It is necessary to describe a DFIG model in the positive and negative sequence reference frames, which is based on stator voltage orientation (SVO). The positive and negative reference frames can be described as [8], [9]:

$$V_{dq}^{+} = V_{\alpha\beta} e^{-j\omega_e t}, \quad V_{dq}^{-} = V_{\alpha\beta} e^{j\omega_e t} \quad (1)$$

$$V_{dq}^{+} = V_{dq}^{-} e^{-2j\omega_e t}, \quad V_{dq}^{-} = V_{dq}^{+} e^{2j\omega_e t} \quad (2)$$

where superscripts (+) and (–) represent the positive and negative sequence reference frames, respectively.

The stator and rotor voltages of an induction machine can be described as:

$$V_{dqs}^{+} = I_{dqs}^{+} R_s + j\omega\psi_{dqs}^{+} + \frac{d\psi_{dqs}^{+}}{dt} \quad (3)$$

$$V_{dqr}^{+} = I_{dqr}^{+} R_r + (\omega_e - \omega_r)\, j\psi_{dqr}^{+} + \frac{d\psi_{dqr}^{+}}{dt} \quad (4)$$

$$\psi_{dqs}^{+} = L_s\, I_{dqs}^{+} + I_{dqr}^{+} L_m \quad (5)$$

$$\psi_{dqr}^{+} = L_r\, I_{dqr}^{+} + I_{dqs}^{+} L_m \quad (6)$$

with $L_s = L_{ls} + L_m$ and $L_r = L_{lr} + L_m$

In addition under voltage unbalance conditions, there is in addition to dq^+ components there is also dq^- components. The stator, rotor and grid current, voltage and flux vectors can be expressed in terms of their respective positive and negative sequence components as [8], [9]:

$$F_{dqs}^{+} = F_{dqs+}^{+} + F_{dqs-}^{+} = F_{dqs+}^{+} + F_{dqs-}^{-} . e^{-2j\omega_e t} \quad (7)$$

$$F_{dqs}^{-} = F_{dqs-}^{-} + F_{dqs+}^{-} = F_{dqs-}^{-} + F_{dqs+}^{+} . e^{2j\omega_e t} \quad (8)$$

where subscripts +, - are the positive and negative sequence components. The *dq* rotor voltage is:

$$V_{dqr}^{+} = I_{dqr}^{+} R_r + j(\omega_e - \omega_r)\sigma L_r I_{dqr}^{+} + \sigma L_r \frac{dI_{dqr}^{+}}{dt} + \frac{L_m}{L_r}\frac{d\psi_{dqs}^{e}}{dt} \quad (9)$$

where $\sigma = 1 - \dfrac{L_m^2}{L_s L_r}$

The first and third terms on the right side of equation (9) are as a result of *dq*-axis current I_{dqr} and dI_{dqr}/dt. The other terms due to I_{dqr} and ψ_{dqs} can be considered as disturbances. In the

synchronous reference frame these equations can therefore be expressed as [[11]]:

$$V_{dqr}^{e+} = V_{dqr}^{e+\prime} + V_{dqr,comp}^{e+} \quad (10)$$

$$\text{where} \quad V_{dqr}^{e+\prime} = \sigma L_r \frac{dI_{dqr}^{e+}}{dt} \quad (11)$$

and

$$V_{dqr,comp}^{e+} = I_{dqr}^{e+} R_r + (\omega_e - \omega_r)\sigma L_r I_{dqr}^{e+} + (\omega_e - \omega_r)\frac{L_m}{L_r}\psi_{dqs}^{e+} \quad (12)$$

Equation (10) allows decoupled performance of the stator voltage oriented control (SVO) of the rotor-side converter. These voltages can be incorporated into the vector control scheme shown in fig. 4 where *PI* controllers are applied to control rotor current and shaft speed. In (11) the term $\frac{dI_{dqr}^{e+}}{dt}$ is the output of the *PI* controller:

$$\frac{dI_{dqr}^{e+}}{dt} = k_p\left(I_{dqr}^{e+*} - I_{dqr}^{e+}\right) + k_i\int\left(I_{dqr}^{e+*} - I_{dqr}^{e+}\right)dt \quad (13)$$

Using the equations for positive and negative sequence voltages and currents the apparent power of the converter can be calculated. The stator output apparent power can be described in the positive sequence reference frame as [[4], [7]]:

$$S = P_S + jQ_S = -\frac{3}{2}V_{dqs}^{+}I_{dqs}^{+*} \quad (14)$$

where the superscript (+) indicates the positive sequence reference frame and $V_{dq}^{+} = V_d^{+} + jV_q^{+}$ and $I_{dq}^{+} = I_d^{+} + jI_q^{+}$.

Equation (14) can be expanded as [[4], [5], [6], [8]]:

$$S = -\frac{3}{2L_s}\begin{pmatrix}\left(V_{dqs+}^{+} + V_{dqs-}^{-}.e^{-j2\omega_e t}\right)\left(I_{dqs+}^{+*} + (I_{dqs-}^{-}.e^{-j2\omega_e t})^*\right) \\ -L_m.\left(V_{dqs+}^{+} + V_{dqs-}^{-}.e^{-j2\omega_e t}\right)\left(I_{dqr+}^{+*} + (I_{dqr-}^{-}.e^{-j2\omega_e t})^*\right)\end{pmatrix} \quad (15)$$

When (15) is multiplied out and expanded in term of *d* and *q* positive and negative terms, the terms for active and reactive power can be obtained as:

$$S = P_s + jQ_s = \left(P_{so\_av} + P_{s\sin 2}\sin(2\omega_s t) + P_{s\cos 2}\cos(2\omega_s t)\right) + j\left(Q_{so\_av} + Q_{s\sin 2}\sin(2\omega_s t) + Q_{s\cos 2}\cos(2\omega_s t)\right) \quad (16)$$

where $P_{so,}$ $P_{s\ sin2,\ and}$ $P_{s\ cos2,}$ are the dc average, sine and cosine terms respectively of twice the network frequency contained in the stator active power.

The stator reactive components are similarly defined. The coefficients of (16) can be described as:

$$\begin{bmatrix}P_{so\_av}\\ Q_{so\_av}\\ P_{s\_\sin 2}\\ P_{s\_\cos 2}\\ Q_{s\_\sin 2}\\ Q_{s\_\cos 2}\end{bmatrix}_o = -\frac{3}{2\omega_e L_s}\begin{bmatrix}V_{ds+}^{+} & V_{qs+}^{+} & V_{ds-}^{-} & V_{qs-}^{-}\\ V_{qs+}^{+} & -V_{ds+}^{+} & V_{qs-}^{-} & -V_{ds-}^{-}\\ V_{qs-}^{-} & -V_{ds-}^{-} & -V_{qs+}^{+} & V_{ds+}^{+}\\ V_{ds-}^{-} & V_{qs-}^{-} & V_{ds+}^{+} & V_{qs+}^{+}\\ -V_{ds-}^{-} & -V_{qs-}^{-} & V_{ds+}^{+} & V_{qs+}^{+}\\ V_{qs-}^{-} & -V_{ds-}^{-} & V_{qs+}^{+} & -V_{ds+}^{+}\end{bmatrix}\left(\begin{bmatrix}V_{ds+}^{+}\\ V_{qs+}^{+}\\ V_{ds-}^{-}\\ V_{qs-}^{-}\end{bmatrix} + \omega_e L_m\begin{bmatrix}I_{dr+}^{+}\\ I_{qr+}^{+}\\ I_{dr-}^{-}\\ I_{qr-}^{-}\end{bmatrix}\right) \quad (17)$$

Because the d^+ axis is aligned with the positive sequence stator voltage vector the *q* axis component $V_{qs+}^{+} = 0$ [9]. In this paper only the real power oscillating components are being investigated and so by allowing $P_{s\_sin2} = 0$ and $P_{s\_cos2} = 0$ in (17) the negative sequence rotor currents can be controlled as:

$$I_{qr-}^{-} = \frac{2.V_{qs-}^{-}}{\omega_e L_m} + \frac{1}{V_{ds+}^{+}}\left(V_{ds-}^{-}I_{qr+}^{+} - V_{qs-}^{-}I_{dr+}^{+}\right) \quad (18)$$

$$I_{dr-}^{-} = -\frac{2.V_{ds-}^{-}}{\omega_e L_m} + \frac{1}{V_{ds+}^{+}}\left(V_{qs-}^{-}I_{qr+}^{+} - V_{ds-}^{-}I_{dr+}^{+}\right) \quad (19)$$

Compensating terms can also be obtained to control torque pulsations. By analysing the equation for torque, a similar analysis can be progressed and compensating currents I_{dr-}^{-} and I_{qr-}^{-} can be obtained to control the sine and cosine torque pulsations T_{s_sin2} and T_{s_cos2}. The electromagnetic torque in a DFIG can be described as [9]:

$$T_e = \frac{3}{2}\frac{p}{L_s\omega_e}\left(V_{dqs}(t).I_{dqr}^{*}(t)\right) = T_{eo\_av} + T_{e\_\sin 2}\sin(2\omega_e t) + T_{e\_\cos 2}\cos(2\omega_e t) \quad (20)$$

The components T_{eo_av} , T_{e_sin2} and T_{e_cos2} can be expanded as:

$$\begin{bmatrix}T_{e\_av}\\ T_{e\_\sin}\\ T_{e\_\cos}\end{bmatrix} = \frac{-3L_m}{2.L_s\omega_e}\begin{bmatrix}-V_{ds+}^{+} & -V_{qs+}^{+} & -V_{ds-}^{-} & V_{qs-}^{-}\\ V_{qs-}^{-} & -V_{ds-}^{-} & V_{qs+}^{+} & -V_{ds+}^{+}\\ V_{ds-}^{-} & V_{qs-}^{-} & -V_{ds+}^{+} & -V_{qs+}^{+}\end{bmatrix}\begin{bmatrix}i_{dr+}^{+}\\ i_{qr+}^{+}\\ i_{dr-}^{-}\\ i_{qr-}^{-}\end{bmatrix} \quad (21)$$

To reduce the torque pulsations the required control currents can be obtained by allowing $T_{s\_sins2} = T_{s\_cos2} = 0$ in (21). The positive and negative sequence rotor control current references can then be obtained as:

$$I_{dr-}^{-} = \frac{1}{V_{ds+}^{+}}\left[V_{qs-}^{-}.I_{dr+}^{+} - V_{ds-}^{-}.I_{qr+}^{+}\right] \quad (22)$$

$$I_{qr-}^{-} = \frac{1}{V_{ds+}^{+}}\left[V_{ds-}^{-}.I_{dr+}^{+} + V_{qs-}^{-}.I_{qr+}^{+}\right] \quad (23)$$

$$I_{dr+}^{+} = \frac{T_{e\_av} 2L_s \omega_e}{3.L_m} - \frac{1}{V_{ds+}^{+}} \left[V_{ds-}^{-}.I_{dr-}^{-} + V_{qs-}^{-}.I_{qr-}^{-} \right] \quad (24)$$

4. Resonant Controller

Methods to control DFIG's during voltage unbalance conditions include parallel current control techniques operated in the positive and negative sequence reference frames to control the respective positive and negative sequence control currents $I_{dqr}^{+}{}_{+}$, $I_{dqr}^{-}{}_{-}$, $I_{dqg}^{+}{}_{+}$ and $I_{dqg}^{-}{}_{-}$ in the rotor side and grid side converters [[8], [9]]. An alternative method is to use a resonant (R) controller in parallel with the PI current controller. The R controller requires less positive and negative sequence decomposition and thus less time delay and errors [13].

According to (7) and (8) it is clear that during conditions of network voltage unbalance conditions the voltage, current and flux all contain both dc values of the positive sequence components and double frequency ($2\omega_e$) ac values of the negative sequence components in the dq^+ reference frame. The dc components are regulated normally by the PI controller however this controller cannot regulate the double frequency components. The negative sequence control currents $I_{dqr}^{-}{}_{-}$ have a frequency of $2\omega_e$ (100 Hz) and to control these currents adequately it is thus necessary to use a controller that is tuned to 100 Hz. A proportional, integral plus resonant ($PI+R$) rotor side current controller can be implemented for directly controlling both the positive and negative sequence components [12], [13]. The voltage reference output of the $PI\&R$ controller can be described as:

$$V_{dqr}^{e+`} = \left(I_{dqr}^{e+*} - I_{dqr}^{e+} \right) \left\{ k_p + \frac{k_i}{s} + k_{iR} \left(\frac{s}{s^2 + s2\omega_c + (2\omega_e)^2} \right) \right\} \quad (25)$$

In the scheme described by (25) ω_e is the resonance frequency of the controller, K_P and K_i are the proportional gain and the integral gains respectively. This controller has a very high gain around the resonance frequency and it eliminates the steady state error between the reference and the measured signal. The width of the frequency band around the resonance point depends on the integral gain value. A small value produces a very narrow band, whereas a large value produces a wider band. The cut-of frequency ω_c in (25) also increases the band-width. The Bode plots of the resonant controller for integral gain Ki_R of 100, 200, 500, 1000 and 2000, ω_c set to 5 and ω_e set to 100Hz is shown in fig. 1. As can be observed this type of controller can achieve a very high gain in a frequency band around the resonance frequency.

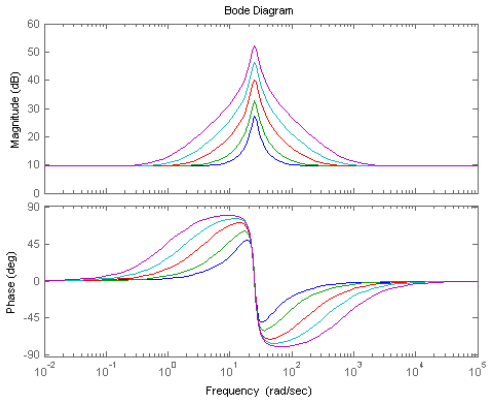

Figure 1: Bode plot of Resonant Controller: Blue is for a k_{iR} gain of 100 whereas purple is for a gain of 2000.

A control scheme incorporating a PI controller in parallel with a resonant (R) controller tuned to twice the network frequency (100 Hz) is implemented as shown in fig. 2. The discrete $PI\&R$ controller shown is implemented in the dq^+ reference frame in the program Matlab/Simulink.

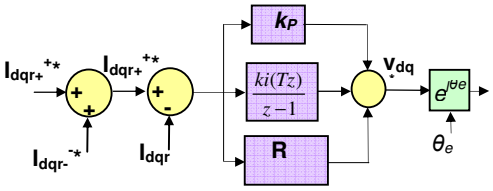

Figure 2: Rotor Side PI and Resonant Controller

The rotor currents are transformed into the positive sequence dq^+ and negative dq^- sequence reference frames, using the rotor slip angle θ_{sl}. Band-stop (notch) filters tuned at $2\omega_e$ are then used to remove the oscillating terms, and leave the respective positive and negative sequence control currents $I_{dqr}^{+}{}_{+}$ and $I_{dqr}^{-}{}_{-}$. The four reference currents $I_{dr}^{+*}{}_{+}$, $I_{qr}^{+*}{}_{+}$, $I_{dr}^{-*}{}_{-}$, and $I_{qr}^{-*}{}_{-}$ are all dc signals separated in the respective positive and negative sequence reference frames as shown in fig 3. The negative sequence components obtained are then incorporated into the positive sequence control loop.

To control the torque pulsations the positive and negative sequence control reference currents, $I_{dr}^{+}{}_{+}$, $I_{dr}^{-}{}_{-}$ and $I_{qr}^{-}{}_{-}$ are obtained form (22), (23) and (24). In this paper reactive power control is not used and the reference $I_{qr}^{+}{}_{+}$ is set = 0.

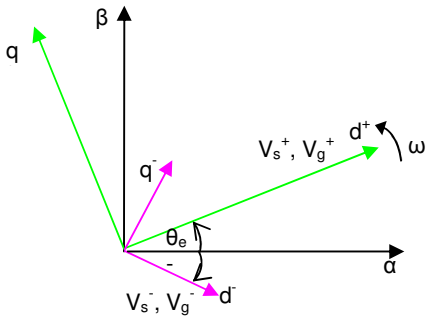

Figure 3: dq Reference Frames

Having obtained the negative sequence components, to use them effectively in the positive sequence current control loop it is necessary to transfer them from the negative sequence reference frame to the positive sequence reference frame. Observing fig. 3, it shows that to align the negative sequence frame onto the positive sequence frame requires a rotation of $2\theta_e$. This transformation is shown in the control loop of fig. 4. Having obtained the negative sequence reference currents in the positive sequence reference frame it is then required to add to the positive sequence reference as shown in fig. 4.

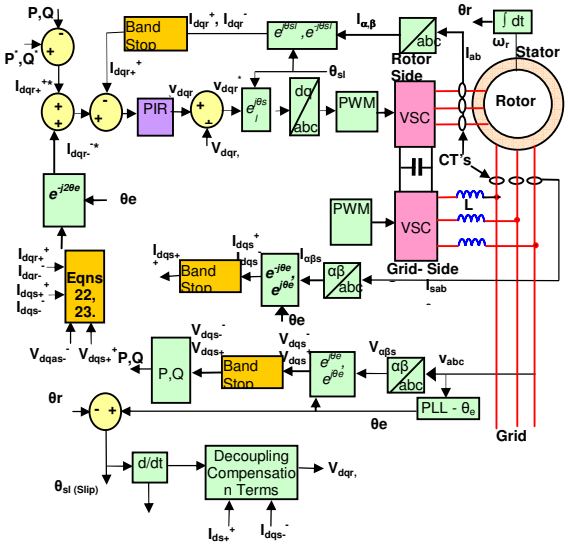

Figure 4: Rotor Side Converter Parallel Unbalance Control Structure

It is also necessary to incorporate positive and negative sequence components, $I_{dqs}{}^{+}{}_{+}$ and $I_{dqs}{}^{-}{}_{-}$ respectively to obtain the necessary decoupling terms, $V_{d\ comp}$ and $V_{q\ comp}$. The control scheme is shown in fig. 4 and further details of the rotor side control scheme can be obtained in [[8]].

5. Grid Side Converter Control

The control structure for the grid-side converter is based on the decoupled *dq* vector control method as previously outlined for the rotor-side converter with SVO. The grid-side converter controls the dc link voltage and can also control reactive power. The *dq* voltage equations can be obtained in the grid/stator voltage synchronous reference frame (SVO) with the d_{axis} aligned with the grid voltage as [[9]]:

$$V^e_{dqg} = I^e_{dqg}R_g + L_g\frac{dI^e_{dqg}}{dt} - \omega_e L_g\, I^e_{dqg} + V^e_{dqg1} \tag{26}$$

Separating (26) into positive and negative sequence components yields:

$$V^+_{dqg+} = I^+_{dqg+}R_g + L_g\frac{dI^+_{dqg+}}{dt} - \omega_e L_g\, I^+_{dqg+} + V^+_{dqg1+} \tag{27}$$

$$V^-_{dqg-} = I^-_{dqg-}R_g + L_g\frac{dI^-_{dqg-}}{dt} - \omega_e L_g\, I^-_{dqg-} + V^-_{dqg1-} \tag{28}$$

The apparent power of the converter can be described as [**Error! Reference source not found.**]:

$$S = P_g + jQ_g = \frac{3}{2}V^+_{dqg}I^{+*}_{dqg} \tag{29}$$

And using (7):

$$S = \frac{3}{2}.\left(\begin{pmatrix}V^+_{dqg+} + V^-_{dqg-}.e^{-j2\omega_e t}\end{pmatrix}.\begin{pmatrix}I^{+*}_{dqg+} + (I^-_{dqg-}.e^{-j2\omega_e t})^*\end{pmatrix}\right) \tag{30}$$

Multiplying (30) and expanding:

$$\begin{aligned}S = \frac{3}{2}\Big\{&\left(V^+_{dg+}.I^+_{dg+} - V^+_{dg+}.jI^+_{dg+} + jV^+_{qg+}.I^+_{dg+} + V^+_{qg+}.I^+_{qg+}\right)\\ &+\left(V^+_{dg+}.I^-_{dg-} - V^+_{dg+}.jI^-_{dg-} + jV^+_{qg+}.I^-_{dg-} + V^+_{qg+}.I^-_{qg-}\right)e^{j2\omega_e t}\\ &+\left(V^-_{dg-}.I^+_{dg+} - jV^-_{dg-}.I^+_{qg+} + jV^-_{qg-}.I^+_{dg+} + V^-_{qg-}.I^+_{qg+}\right)e^{-j2\omega_e t}\\ &+\left(V^-_{dg-}.I^-_{dg-} - V^-_{dg-}.jI^-_{dg-} + jV^-_{qg-}.I^-_{dg-} + V^-_{qg-}.I^-_{qg-}\right)\Big\}\end{aligned} \tag{31}$$

Equation (31) can be equated to:

$$\begin{aligned}P_{acg} &= P_{og} + P_{c2g}\cos(2\omega_s t) + P_{s2g}\sin(2\omega_s t)\\ Q_{acg} &= Q_{og} + Q_{c2g}\cos(2\omega_s t) + Q_{s2g}\sin(2\omega_s t)\end{aligned} \tag{32}$$

The coefficients of (16) can be described as:

$$\begin{bmatrix}P_{og}\\ Q_{og}\\ P_{c2g}\\ P_{s2g}\\ Q_{c2g}\\ Q_{s2g}\end{bmatrix} = \frac{3}{2}\begin{bmatrix}V^+_{dg+} & V^+_{qg+} & V^-_{dg-} & V^-_{qg-}\\ V^+_{qg+} & -V^+_{dg+} & V^-_{qg-} & -V^-_{dg-}\\ V^-_{dg-} & V^-_{qg-} & V^+_{dg+} & V^+_{qg+}\\ V^-_{qg-} & -V^-_{dg-} & -V^+_{qg+} & V^+_{dg+}\\ V^-_{qg-} & -V^-_{dg-} & V^+_{qg+} & -V^+_{dg+}\\ -V^-_{dg-} & -V^-_{qg-} & V^+_{dg+} & V^+_{qg+}\end{bmatrix}\begin{bmatrix}I^+_{dg+}\\ I^+_{qg+}\\ I^-_{dg-}\\ I^-_{qg-}\end{bmatrix} \tag{33}$$

The positive and negative sequence reference currents $I_{dr}{}^{+}{}_{+}$, $I_{qr}{}^{+}{}_{+}$, $I_{dr}{}^{-}{}_{-}$ and $I_{qr}{}^{-}{}_{-}$ are obtained form (33) as:

$$I^{-}_{dg-} = \frac{1}{v^{+}_{dg+}}\left[v^{-}_{dg-}.I^{+}_{dg+} + v^{-}_{qg-}.Ii^{+}_{qg+}\right] \quad (34)$$

$$I^{-}_{qg-} = \frac{1}{v^{+}_{dg+}}\left[v^{-}_{dg-}.i^{+}_{dg+} - v^{-}_{dg-}.i^{+}_{qg+}\right] \quad (35)$$

$$I^{+}_{dg+} = \frac{1}{v^{+}_{dg+}}\left[\frac{2}{3}P_o - V^{-}_{dg-}I^{-}_{dg-} - V^{-}_{qg-}Ii^{-}_{qg-}\right] \quad (36)$$

$$I^{+}_{qg+} = -\frac{1}{V^{+}_{dg+}}\left[\frac{2}{3}Q_o - V^{-}_{qg-}Ii^{-}_{dg-} + V^{-}_{dg-}Ii^{-}_{qg-}\right] \quad (37)$$

6. Grid Side PI&R Control

Equation (26) can be expressed as [[9]]:

$$L_g\frac{dI^{e}_{dqg}}{dt} = V^{e}_{dqg} - I^{e}_{dqg}R_g \;\; - \omega_e L_g \; I^{e}_{dqg} - V^{e}_{dqg1} \quad (38)$$

Similar to the rotor side converter (38) can be incorporated into the vector control scheme shown in Fig. 6 where *PI* controllers are applied to control rotor current and shaft speed. In (38) the term $\frac{dI^{e+}_{dqg}}{dt}$ is the output of the *PI* controller and including the *R* controller the voltage reference output can be described as:

$$V^{e+`}_{dqg} = \left(I^{e+*}_{dqg} - I^{e+}_{dqg}\right)\left\{k_p + \frac{k_i}{s} + k_{iR}\left(\frac{s}{s^2 + s2\omega_c + (2\omega_e)^2}\right)\right\} \quad (39)$$

Third harmonic currents at the grid side converter can also be controlled using an *R* controller tuned to $3\omega_e$ (150Hz) [[12]].
During network voltage unbalance conditions and assuming no zero components the positive and negative sequence of the fundamental frequency and the harmonics at the frequencies of $-2\omega_e$ and $3\omega_e$ are investigated in this paper.
Including the third harmonic components the voltage and current vectors can be expressed in terms of the positive and negative sequence and harmonic components as (7):

$$F^{+}_{dqs} = F^{+}_{dqs+} + F^{-}_{dqs-}.e^{-2j\omega_e t} + F^{3+}_{dqs3+}.e^{2j\omega_e t} \quad (40)$$

$F_{dqs}{}^{3+}{}_{3+}$ refers to the 3rd harmonic components in the positive synchronous reference frame rotating at an angular velocity of $3\omega_e$. The positive, negative and third harmonic reference frames are illustrated in fig. 5. The previously defined negative sequence 2nd harmonic components rotate at a speed of $-2\omega_e$ (angle $-2\theta_e$ - difference between positive axis (d^+) and negative sequence axis (d^-)) and the third harmonic components rotate at a speed of $+2\omega_e$ (angle $2\theta_e$ – difference between 3rd harmonic axis (d^+) and positive axis (d^+)).

From (30) the apparent power including the 3rd harmonic components can be obtained as:

$$S = \frac{3}{2}.\left(\begin{pmatrix}V^{+}_{dqg+} + V^{-}_{dqg-}.e^{-j2\omega_e t} + V^{+3}_{dqg3+}.e^{j2\omega_e t}\end{pmatrix}x \right.$$
$$\left.\begin{pmatrix}I^{+*}_{dqg+} + (I^{-}_{dqg-}.e^{-j2\omega_e t})^{*} + (I^{+3}_{dqg3+}.e^{j2\omega_e t})^{*}\end{pmatrix}\right) \quad (41))$$

Multiplying (40) and expanding yields:

$$S = \frac{3}{2}\left\{\begin{pmatrix}V^{+}_{dqg+}.I^{+*}_{dqg+} + V^{+}_{dqg+}.I^{-*}_{dqg-}\ell^{j2\omega t} \\ + V^{+}_{dqg+}.I^{3+*}_{dqg3+-}\ell^{-j2\omega t}\end{pmatrix}\right.$$
$$+\begin{pmatrix}V^{-}_{dqg-}\ell^{-j2\omega t}.I^{+*}_{dqg+} + V^{-}_{dqg-}.I^{-*}_{dqg-}\ell^{-j2\omega t}\ell^{j2\omega t} + \\ V^{-}_{dqg-}.I^{3+*}_{dqg3+-}\ell^{-j2\omega t}\ell^{-j2\omega t}\end{pmatrix}$$
$$\left.+\begin{pmatrix}V^{3+}_{dqg3+}\ell^{j2\omega t}.I^{+*}_{dqg+} + V^{3+}_{dqg3+}.I^{-*}_{dqg-}\ell^{j2\omega t}\ell^{j2\omega t} + \\ V^{3+}_{dqg3+}.I^{3+*}_{dqg3+-}\ell^{j2\omega t}\ell^{-j2\omega t}\end{pmatrix}\right\} \quad (42)$$

Equation (42) can further expanded and the instantaneous real and reactive powers can then equated to:

$$P_g = \begin{pmatrix}P_{og\_av} + P_{s2g}\sin(2\omega_e t) \\ + P_{c2g}\cos(2\omega_e t) + P_{g\cos 3}\cos(3\omega_e t)\end{pmatrix} \quad (43)$$

$$Q_g = \begin{pmatrix}Q_{go\_av} + Q_{g\sin 2}\sin(2\omega_e t) \\ + Q_{g\cos 2}\cos(2\omega_e t) + Q_{g\cos 3}\cos(3\omega_e t)\end{pmatrix} \quad (44)$$

where since only the real powers are of interest therefore:

$$\begin{bmatrix}P_{og} \\ P_{c2g} \\ P_{s2g}\end{bmatrix} =$$

$$-\frac{3}{2}\begin{bmatrix} V^{+}_{dg+} & V^{+}_{qg+} & V^{-}_{dg-} & V^{-}_{qg-} & V^{3+}_{dg3+} & V^{3+}_{qg3+} \\ \left(V^{-}_{dg-}+V^{3+}_{dg3+}\right) & \left(V^{-}_{qg-}+V^{3+}_{qg3+}\right) & V^{+}_{dg+} & V^{+}_{qg+} & V^{-}_{dg-} & V^{-}_{qg-} \\ \left(V^{-}_{qg-}-V^{3+}_{qg3+}\right) & \left(V^{-}_{dg-}+V^{3+}_{dg3+}\right) & V^{+}_{qg+} & V^{+}_{dg+} & V^{+}_{qg+} & V^{+}_{dg+}\end{bmatrix}\begin{bmatrix}I^{+}_{dg+} \\ I^{+}_{qg+} \\ I^{-}_{dg-} \\ I^{-}_{qg-} \\ I^{3+}_{dg3+} \\ I^{3+}_{qg3+}\end{bmatrix} \quad (45)$$

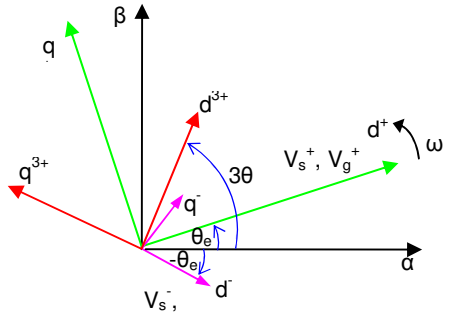

Figure 5: dq 3rd Harmonic Reference Frame

The reference for the active power can be obtained form (45) as:

$$I^{+}_{dg+} = \frac{1}{v^{+}_{dg+}}\left[\begin{array}{l}\frac{2}{3}P_o - V^{-}_{dg-}I^{-}_{dg-} - V^{-}_{qg-}Ii^{-}_{qg-} \\ +V^{3+}_{dg3+}I^{3+}_{dg3+} + V^{3+}_{dg3+}I^{3+}_{dg3+}\end{array}\right] \quad (46)$$

To assist in the control of the third harmonic currents it is necessary to let $P_{c2g} = P_{s2g} = 0$. Thus the reference currents for the 3rd harmonic control in the positive sequence reference frame can be obtained from (45) as:

$$I^{3+}_{dg+} = -\frac{1}{v^{+}_{dg+}}\left[\begin{array}{l}V^{+}_{dg+}I^{-}_{dg-} + \left(V^{-}_{dg-} + V^{3+}_{dg3+}\right)I^{+}_{dg+} \\ +\left(V^{-}_{qg-} + V^{3+}_{qg3+}\right)I^{+}_{qg+}\end{array}\right] \quad (47)$$

$$I^{3+}_{qg+} = -\frac{1}{v^{+}_{dg+}}\left[\begin{array}{l}V^{+}_{dg+}I^{-}_{qg-} + \left(V^{-}_{qg-} - V^{3+}_{qg3+}\right)I^{+}_{dg+} \\ -\left(V^{-}_{dg-} - V^{3+}_{dg3+}\right)I^{+}_{qg+}\end{array}\right] \quad (48)$$

The voltage reference output of the *PI&R* controllers will then be as:

$$V^{e+`}_{dqg} = \left(I^{e+*}_{dqg} - I^{e+}_{dqg}\right)\left\{\begin{array}{l}k_p + \frac{k_i}{s} + k_{iR}\left(\frac{s}{s^2 + s2\omega_c + (2\omega_e)^2}\right) \\ +k_{iR}\left(\frac{s}{s^2 + s2\omega_c + (3\omega_e)^2}\right)\end{array}\right\} \quad (49)$$

7. Coordinated Control

Arguably the most serious effects that voltage unbalance has on DFIG's is torque pulsations followed by stator power oscillations and rotor current oscillations. Coordinated control involves the modification of the control structure of the grid side converter so that the power oscillations produced at the stator of the DFIG are reduced at the DFIG terminals.

The idea behind coordinated control is to use the rotor side converter and the grid side converter in a coordinated way so that the primary concern of the rotor side converter is to control the torque pulsations and the grid side converter can then assist in controlling the total power oscillations. Due to the limitations of the control variables it is not possible to control stator power oscillations and the torque pulsations concurrently using the rotor side converter, it is only possible to either control the stator power oscillations or the torque pulsations [[9]]. The stator delivers more real power than the grid side and the power oscillations due to voltage unbalance are greater on the stator side. The total apparent power of a DFIG is [[6]]:

$$S = P_T + jQ_T = -\frac{3}{2}\left(V^{+}_{dqs}I^{*}_{dqs} + V^{+}_{dqr}I^{*}_{dqr}\right) \quad (50)$$

The total real power in equation (50) is $P_T = Ps + P_g$. From (16) and (32) and knowing that $S_g = P_g + jQ_g$ the total real power can be described as:

$$\begin{array}{l}P_T = \left(P_{s\_av} + P_{s\_\sin 2}\sin(2\theta_e) + P_{s\_\cos 2}\cos(2\theta_e)\right) \\ \quad + \left(P_{og} + P_{s2g}\sin(2\theta_g) + P_{c2g}\cos(2\theta_g)\right)\end{array} \quad (51)$$

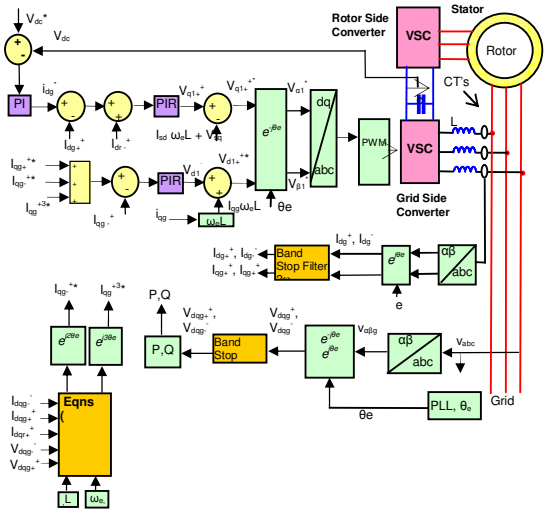

Figure 6: Grid Side Converter Control

The rotor side converter and the grid side converter are both controlled in the grid/stator voltage reference frame, see fig. 2 and therefore $\theta_e = \theta_g$ and (51) can be described as:

$$\begin{array}{l}P_T = (P_{s\_av} + P_{og}) + (P_{s\_\sin 2} + P_{s2g})\sin(2\theta_e) \\ \quad + (P_{s\_\cos 2} + P_{c2g})\cos(2\theta_e t)\end{array} \quad (52)$$

If in (52) letting $P_{s\_sin2} = -P_{s2g}$ and $P_{c\_cos2} = -P_{c2g}$ then the total real power becomes $P_T = (P_{s\_av} + P_{og})$. Observing (33) and (17) and with the rotor side converter *d*-axis aligned with stator/grid voltage and the grid side converter *d*-axis also aligned with the grid voltage will result in $V_{qs}^{+}{}_{+} = V_{qg}^{+}{}_{+} = 0$ and letting $P_{s2g} = -P_{s\_sin2}$, yields:

$$\begin{array}{l}P_{s2g} = \frac{3}{2}\left(V^{-}_{qg-}I^{+}_{dg+} - V^{-}_{dg-}I^{+}_{qg+} - 0 + V^{+}_{dg+}I^{-}_{qg-}\right) = \\ \left\{-P_{s\_\sin 2} = \frac{3}{2\omega_e L_s}\left(V^{-}_{qs-}V^{+}_{ds+} + 0 + 0 + V^{+}_{ds+}V^{-}_{qs-}\right)\right. \\ \left. -\frac{3L_m}{2L_s}\left(V^{-}_{qs-}I^{+}_{dr+} - V^{-}_{ds-}I^{+}_{qr+} + 0 + V^{+}_{ds+}I^{-}_{qr-}\right)\right\}\end{array} \quad (53)$$

And solving (53) to get the grid side I_{qg}^{-}:

$$\begin{array}{l}I^{-}_{qg-} = \frac{1}{V^{+}_{dg+}}\left[-V^{-}_{qg-}I^{+}_{dg+} + V^{-}_{dg-}I^{+}_{qg+}\right] + \frac{2}{\omega_e L_s V^{+}_{dg+}}\left(V^{-}_{qs-}V^{+}_{ds+}\right) \\ -\frac{L_m}{L_s V^{+}_{dg+}}\left(V^{-}_{qs-}I^{+}_{dr+} - V^{-}_{ds-}I^{+}_{qr+} + V^{+}_{ds+}I^{-}_{qr-}\right)\end{array} \quad (54)$$

Similarly For $P_{s\_cos2} = -P_{c2g}$, from (17) and (33):

$$P_{s\_\cos 2} = \left\{ \begin{array}{l} -\frac{3}{2\omega_e L_s}\left(V^-_{ds-}V^+_{ds+} + 0 + V^+_{ds+}V^-_{ds-} + 0\right) \\ \quad + \frac{3L_m}{2L_s}\left(V^-_{ds-}I^+_{dr+} + V^-_{qs-}I^+_{qr+} + V^+_{ds+}I^-_{dr-} + 0\right) \end{array} \right\}$$

$$= -P_{c2g} = -\frac{3}{2}\left[V^-_{dg-}.I^+_{dg+} + V^-_{qg-}.I^+_{qg+} + V^+_{dg+}.I^-_{dg-} + 0\right] = 0 \quad (55)$$

And solving (55) to get the grid side negative sequence I_q control reference yields:

$$I^-_{dg-} = -\frac{1}{V^+_{dg+}}\left[V^-_{qg-}.I^+_{dg+} + V^-_{dg-}.I^+_{qg+}\right] + \frac{2}{V^+_{dg+}\omega_e L_s}\left(V^+_{ds+}V^-_{ds-}\right) - \frac{L_m}{V^+_{dg+}L_s}\left(V^-_{ds-}I^+_{dr+} + V^-_{qs-}I^+_{qr+} + V^+_{ds+}I^-_{dr-}\right) \quad (56)$$

8. Simulation Results

The DFIG wind turbine in this study is modelled in Matlab/Simulink [[2]] to analyse the behaviour of the DFIG to grid voltage unbalance.

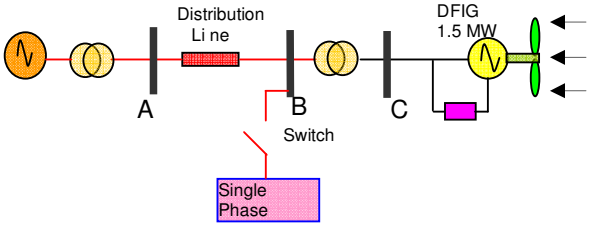

Figure 7: DFIG and Network Model

The system under investigation is illustrated in fig. 7 and further details can be obtained in [[8]]. As shown in fig. 5 a single-phase load on the primary side of the distribution transformer is supplied at bus B. The DFIG is rated at 1.5 MW and the parameters are tabulated in Table 1 Appendix A. The network and DFIG illustrated in fig. 7 and the control scheme associated with the DFIG were implemented in a model in the software program Matlab/Simulink. The switching frequency for both the grid side and rotor side converters is set to 4kHz. Variation in rotor speed is not of concern in this paper and therefore the speed is set to a fixed value of 1.2 pu and an input torque value of 0.8 pu.

A timed switch introduces a single-phase load at 0.5s (fig. 7). In the model when the switch is closed this single-phase load introduces a voltage unbalance of 6% at Bus B, and observed in fig. 8(a). The voltage unbalance is expressed as the ratio of the negative sequence voltage to the positive sequence voltage [[3]]. Fig. 8(b) also shows the current unbalance in the region of 17% at bus B. The current unbalance can be many multiples of the voltage unbalance in induction machines [[3]]. When the compensation scheme is introduced in the rotor side converter the improvement in the current unbalance at the DFIG terminals is evident in Fig. 8(c), with a reduction form 17% to about 4%.

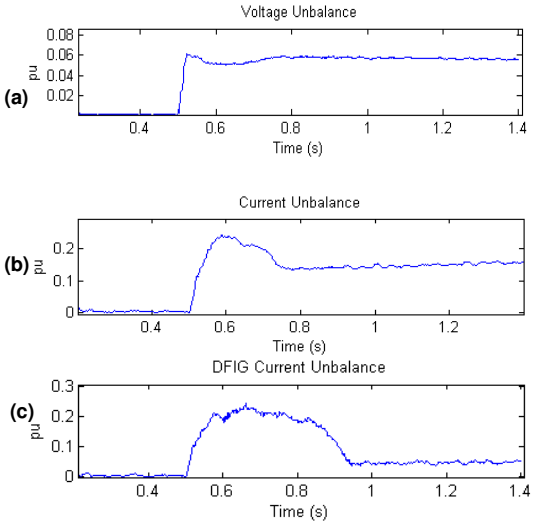

Figure 8: Unbalanced Voltage and Current at Bus B

The control schemes of the rotor side and grid side converters are set as follows: the rotor side converter is configured to control the power delivered to the grid depending on the input power reference and also to control the torque pulsations i.e. using (22) and (23). The grid side converter is configured to control the dc link voltage at 1200V and coordinated with the rotor side converter to control the DFIG total power oscillations.

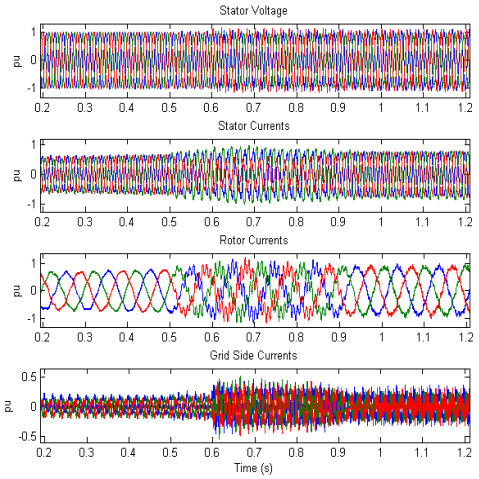

Figure 9: Stator Voltage & Stator and Rotor Currents

The stator voltage can be observed in fig. 9 and is clearly unbalanced when the network becomes unbalanced at 0.5s. The stator, rotor

and grid side currents can also be observed in fig. 9. The stator and rotor currents become very unbalanced at 0.5s and when the rotor side converter compensation is introduced at 0.6s they start to reduce and are eliminated at about 0.9S. The rotor currents have a frequency of 10Hz (rotor speed 60Hz – grid frequency 50Hz). Due to the negative sequence rotation as a result of voltage unbalance, the induced oscillations in the rotor have a frequency 110 Hz (60 Hz + 50 Hz) and oscillations are clearly visible starting at 0.5s in fig. 9.

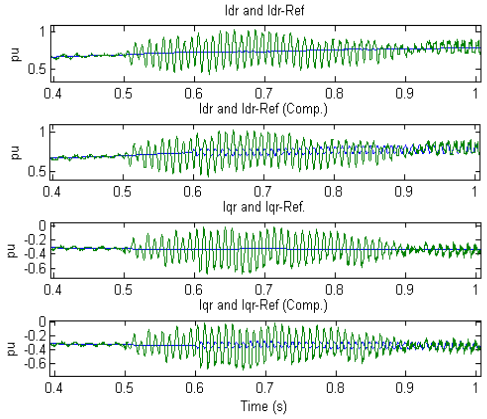

Figure 10: Rotor Side Converter Idr and Iqr currents

The measured three phase rotor currents are transformed into the dq^{+} reference frame, and when subjected to network voltage unbalance conditions will result in an ac component of the negative sequence at $2\omega_e$ super-imposed on the dc component of the positive sequence. The rotor side converter reference currents I_{dr}^{*} (I_{dr}-Ref) and I_{qr}^{*} (I_{qr}-Ref) and the actual currents I_{dr}- and I_{qr}- before and after compensation is applied, are plotted in fig. 10. It is clear form the plots that when compensation is introduced the actual currents I_{dr} and I_{qr} follow the reference currents Idr* (I_{dr}-Ref) and I_{qr}^{*} (I_{qr}-Ref) closely.

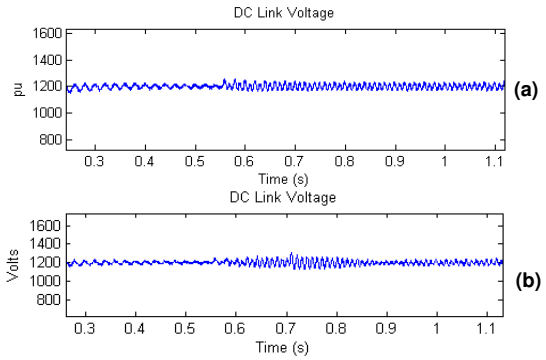

Figure 11: DC Link Voltage (Top-Standard Control)

Fig. 11 shows a plot of the dc link voltage with the standard control scheme Fig 11(a) and when the grid side compensation scheme is introduced Fig. 11(b). There is some reduction in the amplitude of the voltage oscillations.

Fig. 12(a) shows the stator power plot with stator power oscillations when unbalance is introduced and fig. 12(b) when compensation is introduced. Due to the step nature of the introduction of the single-phase load there is a period of about 0.2 s before the DFIG system reaches a steady state with constant power oscillations. When the compensation scheme is introduce at 0.6s the oscillations are dramatically reduced at about 0.8 s, fig. 12(b), compared to the standard control technique Fig. 12(a).

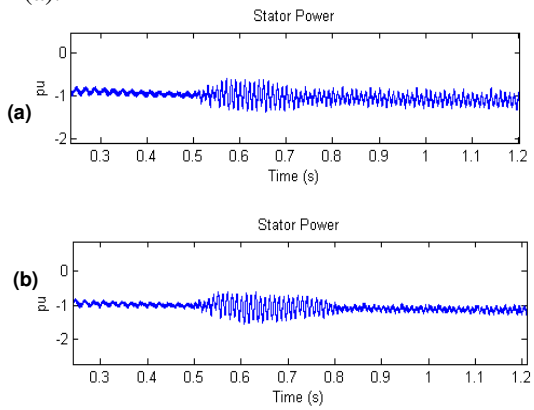

Figure 12: Stator Power (Top-Standard Control-Bottom Compensation)

Fig. 13 is a plot of the DFIG torque with the DFIG input torque set-point set to 0.8 pu. When the voltage compensation is introduced at 0.6 s the oscillations are dramatically reduced as shown in Fig. 13(b).

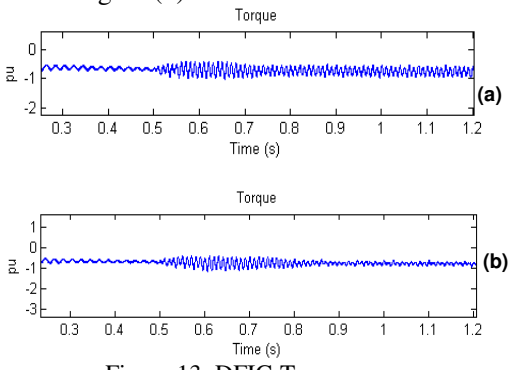

Figure 13: DFIG Torque

Plots of the grid side power are shown in Fig. 14. The grid side converter is controlled to reduce the total power oscillations at the DFIG terminals. There is a good reduction of the grid side converter power oscillations.

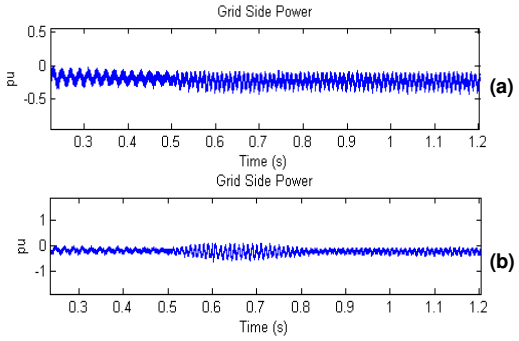

Figure 14: Grid Side Power

The total power delivered by the DFIG to the grid from both the stator and rotor is plotted in fig. 15. There is a good reduction in the power oscillations as a result of the grid side converter configured to assist in reducing the overall power oscillations.

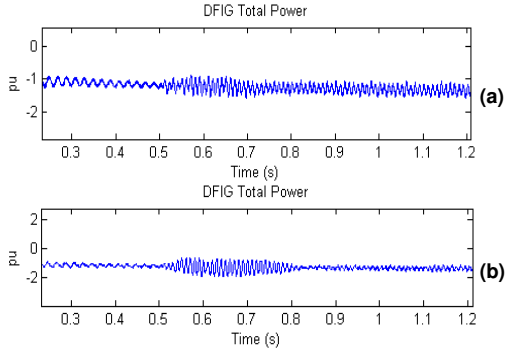

Figure 15: Grid Side Power

To alleviate the 3rd harmonic currents at the grid side converter and rotor side converter (47) and (48) are introduced to the *PI&R* current controllers in the grid side converter. Fig. 16 and fig. 17 show plots of the 3rd harmonic currents at the terminals of the DFIG and at the grid side converter. When the voltage unbalance is introduced at 0.5 s the third harmonic currents rise to about 3%. When the resonant controller is introduced at 0.6 s the 3rd harmonic currents reduce to about 1%.

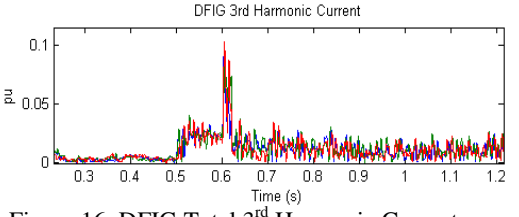

Figure 16: DFIG Total 3rd Harmonic Currents

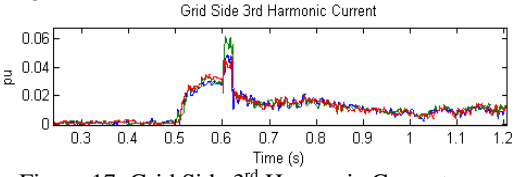

Figure 17: Grid Side 3rd Harmonic Currents

9. Conclusion

A resonant control structure to improve and mitigate the detrimental effects of voltage unbalance on a DFIG rotor-side and grid-side converter was investigated. In particular modifications to the control structures of both the rotor side and the grid side converters was implemented to reduce the pulsations in the torque and the total power oscillations on the DFIG. The results of the simulations performed in Matlab/Simulink of the simple network model show that the pulsations due to torque are practically eliminated and the total power oscillations at the DFIG terminals are significantly reduced.

In addition it was also shown that the resonant controller can also be incorporated to control third harmonic currents generated by the grid side converter.

10. Appendix A

V_{dqs}^{+}, V_{dqs}^{-} = Stator dq voltages in the positive and negative sequence reference frames.

I_{dqs}^{+}, I_{dqs}^{-} = Stator dq currents in the positive and negative sequence reference frames.

I_{dqr}^{+}, I_{dqr}^{-} = Rotor dq currents in the positive and negative sequence reference frames.

ψ_{dqs}^{+}, ψ_{dqs}^{-} = Stator dq flux linkages in the positive and negative sequence reference frames

ψ_{dqr}^{+}, ψ_{dqr}^{-} = Rotor dq flux linkages in the positive and negative sequence reference frames

R_s, L_s = Stator winding resistance and inductance

L_m = Magnetising inductance.

$R_r^{`}$, $L_r^{`}$ = Rotor referred winding resistance and inductance

R_g, L_g = Grid side filter resistance and inductance

L_{ls}, L_{lr} = Stator and rotor leakage inductance

ω_e = Grid angular velocity

11. Appendix B DFIG Simulink Parameters

Rated Power	1.5MW	R_r	0.005 pu
Frequency	50 Hz	L_{lr}	0.156 pu
Rated Voltage	575V	L_m	2.9 pu
R_s	0.00706 pu	Inertia Constant	5.04s
L_{ls}	0.171 pu	Stator/Rotor turns ratio	0.38

Table 1: Simulink Control Parameters.

	Rotor Side	**Grid Side**
Kp	2.5	3
Ki	30	400
KiR	1000	1000

Resonant Controllers: $R = \frac{sk_{ir}}{s^2+2s\omega_c+(2.2\pi.50)^2} = \frac{z.0.499382.10^{-4}+0+0.499382.10^{-4}}{z^2-z.1.995557+0.9995}$

References

[1]. A Larson, The Power Quality of Wind Turbines, PhD. Dept. of Electrical Power Engineering, Chalmers University of Technology, Gothenburg, Sweden 2000.

[2]. Matlab. The Mathworks Inc.

[3]. M.F. Conlon and J. Kearney, "Negative Sequence Analysis of Induction Machines" in Proc. *40th Universities Power Engineering Conference (UPEC)*, Cork, Ireland, 6th - 9th September 2005

[4]. Lie Xu, Yi Wang, "Dynamic Modelling and Control of DFIG-Based Turbines Under Unbalanced Network Conditions", IEEE Transactions on Power Systems, 2007. pp 314-323.

[5]. Yi Wang, Lie Xu, "Control of DFIG-Based Wind Generation Systems under Unbalanced Network Supply", in Proc. *Machines and Drives Conference, 2007, IEMDC* 3-5th May '07. pp", IEEE International, Electrical 430-435.

[6]. Jeong-Ik Jang, Young-Sin Kim, "Active and Reactive Power Control of DFIG for Wind Energy Conversion under Unbalanced Grid Voltage", in Proc. *IEEE IPEMC Conference* 2006.

[7]. Hu Jia-bing, He Yi-kang, "Enhanced control of DFIG-using back-to-back PWM VSC under unbalanced grid voltage conditions", Journal of Zhejiang University SCIENCE A, China, 2007. pp 1330-1339.

[8]. J Kearney, M. F. Conlon, "Control of Double-Fed Induction Generator Wind Turbine During Network Voltage Unbalance Conditions", in Proc. *42nd Universities Power Engineering Conference (UPEC),* Padua, Italy, 2nd - 5th September 2008.

[9]. J Kearney, M. F. Conlon, "The Integrated Control of the Rotor Side and Grid Converters in a DFIG to Reduce Both Power and Torque Pulsations During Network Voltage Unbalance Conditions", in Proc. *43nd Universities Power Engineering Conference (UPEC),* Glasgow, Scotland, 1nd - 4th September 2009.

[10]. Lie XU, "Coordinated Control of DFIG's Rotor and Grid Side Converters During Network Unbalance", IEEE Transactions on Power Electronics, vol. 23, no. 3, May 2008.

[11]. S. K. Salman, Babak Badrzadeh, "New Approach for Modelling Doubly-Fed Induction Generator (DFIG) for grid-connection studies", …

[12]. Jia-bing Hu, Wei Zhang, Hong-sheng Wang, He Yi-kang Lie Xu, "Proportional integral plus multi-frequency resonant current controller for grid-connected voltage source converter under imbalanced and distorted supply voltage conditions", IEEE Journal of Zhejiang University SCIENCE A, 2009, ISSN 1862-1775.

[13]. Jia-bing Hu, Yi-kang Lie Xu, "Modelling and enhanced control of DFIG under unbalanced grid voltage conditions", Electrical Power Systems Research 79, 2009, pp 273-281.